Available online at www.sciencedirect.com
SCIENCE DIRECT®
International Journal of Mass Spectrometry 234 (2004) 1–9
International Journal of Mass Spectrometry
www.elsevier.com/locate/ijms

Activation of protonated peptides and molecular ions of small molecules using heated filaments in Fourier-transform ion cyclotron resonance mass spectrometry

Richard L. Wong, Errol W. Robinson, Evan R. Williams*

Department of Chemistry, University of California, Latimer Hall 1460, Berkeley, CA 94720, USA

Received 22 September 2003; accepted 4 December 2003

In celebration of Alan G. Marshall's 60th birthday and in appreciation for his wonderful contribution to instrumentation, methods development, theory, and application in FT-ICR and beyond.

Available online 16 January 2004

Abstract

A new apparatus that uses heated filaments to dissociate ions in Fourier-transform ion cyclotron resonance mass spectrometry is described. With this apparatus, molecular ions of both acetophenone and *n*-butylbenzene can be dissociated very rapidly. A plot of the natural log of the dissociation rate constant versus inverse radiant temperature yields a straight line from which an Arrhenius activation energy is obtained. From this value, the threshold dissociation energy can be estimated. For acetophenone, we find a value that is within the range of previously measured values. However, for *n*-butylbenzene, the calculated threshold dissociation energy value is too high. We attribute this result, and the appearance of a higher energy dissociation product, to the absorption of visible photons produced at the high filament temperatures used, a factor not currently included in our modeling. In contrast to the small ions, larger peptide ions do not undergo significant dissociation with the current apparatus. The "effective" internal temperature of the larger ions can be measured by using the heated filaments in combination with blackbody infrared radiative dissociation. The "effective" temperature of the peptide ions is increased substantially less than that for the smaller ions.

Keywords: BIRD; Graybody; Filaments dissociation; Dissociation kinetics; FT-ICR

1. Introduction

The ability to dissociate ions for structural characterization using infrared radiation is well established [1–23]. In trapping mass spectrometers, this can be done with either pulsed [1,2] or continuous lasers at specific wavelengths [3–7], or with a blackbody source which produces photons distributed over a broad range of wavelengths [8–14]. For the former, low power cw CO_2 lasers have been primarily used. This infrared multiphoton dissociation (IRMPD) method has been applied to important problems in isomeric ion structure differentiation [7], biomolecule sequencing and identification [15], and the study of ion energetics [17–23]. The use of lasers for these applications has the advantages that the photons can be pulsed and large amounts of internal energy can be deposited into an ion so that even very stable ions can be readily dissociated. It is possible to extract information about the dissociation energetics from these experiments by measuring dissociation kinetics as a function of laser power [17–23]. Because this is a relatively "slow" heating method in which sequential absorption of IR photons raises the internal energy of the ion with time, low-energy dissociation pathways are primarily observed.

The use of blackbody radiation has some advantages over IR laser photodissociation. The broad Planck distribution enables absorption over a wide range of frequencies, and the energy deposition into an ion can be very well characterized with this method [8–14]. This makes possible extracting information about dissociation energetics from both small and large ions with high accuracy [8–14]. Because of the temperatures that are readily accessible by heating a vacuum chamber, the blackbody radiation field is primarily in the infrared region. This has led to the name of this technique of blackbody infrared radiative dissociation or BIRD [9]. However, very stable ions often do not dissociate at

* Corresponding author. Tel.: +1-510-643-7161.
E-mail address: williams@cchem.berkeley.edu (E.R. Williams).

1387-3806/$ – see front matter © 2003 Elsevier B.V. All rights reserved.
doi:10.1016/j.ijms.2003.12.003

the temperatures readily accessible in current experimental apparatus, and the method has not been used in a pulsed manner due to the large thermal mass of the heated areas.

Near blackbody radiation can be obtained using a heated filament, and several implementations have used a heated filament as a source of photons for dissociation [24–29]. This technique has the advantage of being a pulsed method, like IRMPD and a broadband photon source similar to BIRD.

Sena and Riveros were the first to implement a filament dissociation apparatus in a Fourier-transform ion cyclotron resonance (FT-ICR) mass spectrometer [24]. In this pioneering experiment, a tungsten filament was attached outside their ion cell located approximately 0.5 cm from a partially open detection plate. They studied the dissociation of acetophenone molecule ions and found an Arrhenius relationship between the dissociation rate constant and the radiation temperature of the heated filament ($\log_e k_{diss}$ versus $1/T_{rad}$) which was varied over a range from 910 to 1700 K. From modeling these data, they were able to obtain a value for the threshold dissociation energy which fit within the wide range of values that had been measured previously with other methods [24]. Subsequent work by Sena and Riveros examined the keto-enol isomerization of acetophenone [25] and 2′-methylacetophenone molecular ions [26] using this method. The threshold dissociation energy for loss of methyl from the molecular ion of *p*-cymene has also been obtained from this filament dissociation method [27].

Russell and coworkers have also implemented a heated filament ion cell in FT-ICR which uses a heated tungsten wire that runs through the symmetry axis of a cylindrical ion cell [28]. This geometry has the advantage of close proximity of the ions to the heated filament. Filament temperatures as high as 950 K were reported. The dissociation of benzyl chloride was investigated and evidence for isomerization was reported.

Janaway and Brauman used a heated filament device to perform photoelectron detachment of NO^- [29]. In this apparatus, a rhenium filament was mounted just outside a 1 cm diameter hole of one of the trapping plates. The observed k_{diss} for the loss of NO^- had both pressure dependent and independent components. The latter was attributed to photodetachment induced by the light emitted from the heated filament.

Here, we present data from a new apparatus for filament dissociation that has the capability for much higher photon flux than previous experiments. The dissociation of molecular ions of acetophenone and *n*-butylbenzene as well as two small protonated peptides are investigated. We find that although this device is very efficient for dissociating small ions, larger ions are not readily dissociated. We attribute the high dissociation efficiency for small molecules to effects of the visible photons that are produced at the high filament temperatures. These results have implications for obtaining threshold dissociation energies from filament dissociation data of small ions and also for obtaining structural information for larger ions using this technique.

2. Experimental section

2.1. Mass spectrometry

Experimental measurements were performed on a 2.7-T FT-ICR mass spectrometer using either an electron impact ionization source that produces ions internal to the ion cell or an external electrospray ionization source. The electron ionization source is placed 60 cm from the ion cell and aligned to the opening of the rear trap plate. Acetophenone and *n*-butylbenzene are introduced into the vacuum chamber through a gas inlet system connected to a piezoelectric pulsed valve that is opened for 0.3–0.5 s to allow sample to enter the vacuum chamber. Samples are degassed using several freeze-pump-thaw cycles. Molecular ions of acetophenone and *n*-butylbenzene are produced by electron impact (∼15 eV electrons) during and after the introduction of the reagent gas for a total duration of 1.5–2.0 s. Protonated peptides are generated using nanoelectrospray ionization. Nanoelectrospray needles are made from 1.0 mm outer diameter borosilicate capillaries that are pulled to a tip inner diameter of ∼4 μm using a micropipette puller (Sutter Instruments Inc., Novato, CA). Ions formed by electrospray are directed into the ion cell through five stages of differential pumping with a series of ion lens. Dry nitrogen gas is introduced into the vacuum chamber using a piezoelectric pulsed valve during ion accumulation to improve the trapping efficiency and to enhance thermalization of the trapped ions.

High temperature near-blackbody radiative photons are generated using two "heated filament units." Each unit is composed of three tungsten filaments of 3 cm in length (0.0025 cm × 0.076 cm, W340, Scientific Instruments Service, Ringoes, NJ), and the two ends of the tungsten filaments are spot welded to two stainless steel electrodes (Fig. 1a). Each electrode is attached to a macor block and together placed on a stainless steel plate. A piece of woven copper mesh is attached to the stainless steel plate and is not connected to either the electrode or the filaments. The macor blocks electrically insulate the filaments and the electrodes from the rest of the instrument (Fig. 1a). Electric potentials are applied to the two electrodes to generate electric current through the filaments, causing them to resistively heat and emit photons. The filaments are only heated during the ion reaction delay.

The two heated filament units are placed in two gaps (2.7 cm wide) between the excite/detect plates, with the copper mesh side facing the interior of the ion cell (Fig. 1b). The copper mesh shields the ion cell interior from the electric potential of the tungsten filaments, while allowing ∼25% of the photons to pass through to the cell center. For most of the experiments, the filaments were offset to a small positive potential (+1 − 5 VDC) with respect to the copper mesh to ensure that any electrons produced by the heated filaments would not be accelerated towards the center of the ion cell. Tests were performed periodically to ensure that the heated filaments did not

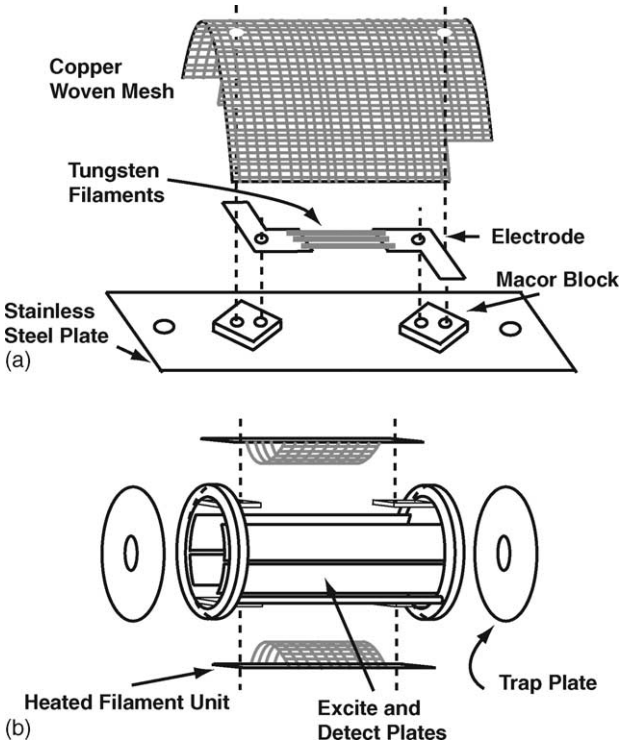

Fig. 1. Schematic diagrams of (a) a single heated filament unit, and (b) the cylindrical ion cell with the two heated filament units.

generated ions inside the ion cell through electron impact ionization.

This new FT-ICR ion cell was set inside a thermal copper jacket. A detailed description of the thermal jacket is reported elsewhere [30]. Since the ion cell and the thermal jacket are in close proximity to the tungsten filaments, heat is transferred to the ion cell and to the thermal jacket when the tungsten filaments are heated. The temperature of the thermal jacket rose from room temperature (∼22 °C) to as high as 35 °C. Tests were performed to demonstrate that ions of interest did not dissociate inside a 35 °C thermal jacket without the filaments being heated. The photon emission from the thermal jacket at 35 °C is minor compared to that from the heated filaments.

2.2. Materials

Acetophenone and *n*-butylbenzene were obtained from Aldrich Company (Milwaukee, WI) and AlfaProducts (Danveus, MA), respectively. Leucine enkephalin and bradykinin were purchased from Sigma Chemical Company (St. Louis, MO) and used as they are. Leucine enkephalin and bradykinin were electrosprayed from 1×10^{-3} M aqueous solution.

2.3. Modeling

Conformational searches to find the low energy structures of acetophenone and *n*-butylbenzene molecular ions are performed with 1000 internal coordination Monte Carlo search steps, with the structures subsequently energy minimized using the MMFFs force field in the Maestro 3.0 suite of programs (Schrödinger Inc., Portland, OR). For acetophenone, only one structure is identified. For *n*-butylbenzene, the lowest energy conformation is found 130 times out of the 1000 search steps. Each of the lowest energy structures for acetophenone and *n*-butylbenzene is further energy minimized at the RHF/6-31G** level using Jaguar 4.0 (Schrödinger Inc., Portland, OR). Vibrational frequencies and their corresponding infrared intensities are calculated from the resulting energy minimized structure at the same computational level.

Dissociation threshold energies (E_o) are determined from the experimentally measured values of Arrhenius activation energy (E_a) via master equation modeling. E_o values that result in a fit to the measured E_a values within one standard deviation are determined. Because the radiation power from a filament at temperature (T_{rad}) is lower than that from a true blackbody source, neither the experimental frequency factors (A) nor the absolute values of the dissociation rate constants (k_{diss}) are included in the fitting procedure. The transition state vibration frequencies are altered to generate a wide range of high-pressure frequency factors (A^{∞}) ranging from 10^9 to 10^{17} s^{-1}.

3. Results and discussion

3.1. Filament temperature

The photon distribution in the center of the ion cell is a combination of photons emitted from the filaments, from the rest of the cell, and from the surrounding thermal copper jacket. The effect of photons entering from outside the thermal jacket is negligible [30]. Because the heated filaments only consist of a small fraction of the emission surface, the photon intensity experienced by the ions is lower than that at the surface the heated filaments. Sena and Riveros have reported that the slope of an Arrhenius plot varies by less than 10% even when the photon intensity from the filament to the ions is attenuated by as much as 94% [24,27]. In other words, the E_a values extracted from Arrhenius plots are largely insensitive to significant attenuation of photon flux. E_a values are extrapolated based on the radiation temperature of the tungsten filaments (T_{rad}), not the true filament temperature (T_{fil}) [24]. The radiation temperature is the blackbody temperature at which the total emission power is equivalent to the integrated power from the tungsten filament [31]. The value of T_{rad} is calculated from T_{fil} [31].

Three approximations are made in analyzing our data to obtain T_{fil}. First, all six of the tungsten filaments are expected to change their resistivity at the same rate because all have similar lengths (within 10%). Second, the change in resistivity is assumed to be entirely due to the tungsten filaments because the filaments have much greater resistance per length than the rest of the circuit; hence, most power

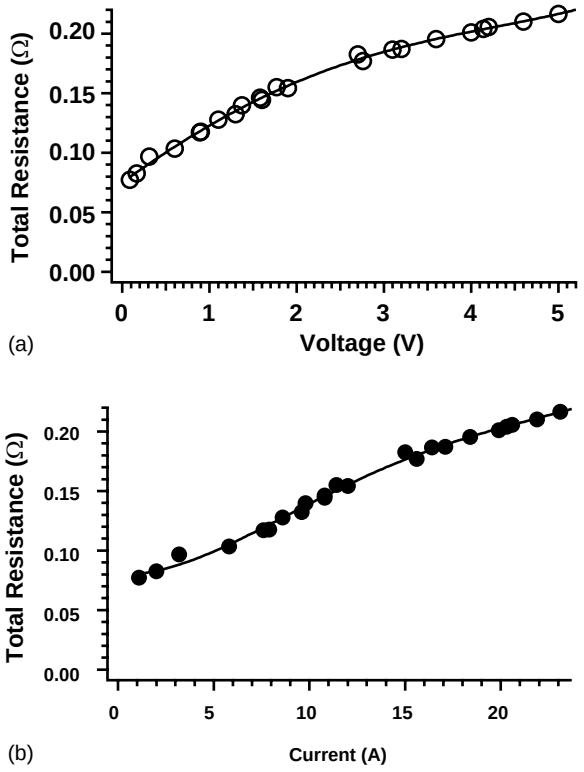

Fig. 2. The resistance of the entire heating circuit plotted as a function of (a) the applied electric potential (open circles), and (b) the applied electric current (solid circles).

dissipates through the tungsten filaments rather than through the rest of the electrical circuit at high current. The resistance of the rest of circuit is expected to be roughly constant. The third approximation is a simplification by defining a uniform temperature to the filaments. In practice, the ends of a filament are closer to the mounts, and therefore the ends are cooler than the center of filament due to thermal conduction. Because the filaments are only heated during the ion dissociation period, the value of T_{fil} at very short reaction times (<1 s) will be overestimated.

The temperature of a tungsten filament, T_{fil} (K), can be calculated from its resistivity, ρ ($\mu\Omega$ cm), using the following expression [24,31]:

$$T_{\text{fil}}(\text{K}) = 103.898 + 38.04\rho - 0.0938\rho^2 + 0.000024\rho^3 \quad (1)$$

The resistivity is determined from the resistance and the dimensions of the filaments. During each experiment, the resistance of the entire circuit is obtained by measuring the voltage across and the current through the circuit. Because the tungsten filaments are not the only sources of resistance, the remaining internal resistance is subtracted out before calculating the resistivity of the filaments.

In Fig. 2a and b, the resistance of the entire circuit is plotted against voltage and current, respectively. A fourth-order polynomial functional is used to fit both sets of data. The resistance of the entire circuit at room temperature is determined to be $0.0775 \pm 0.0005\,\Omega$ from the *y*-intercepts of

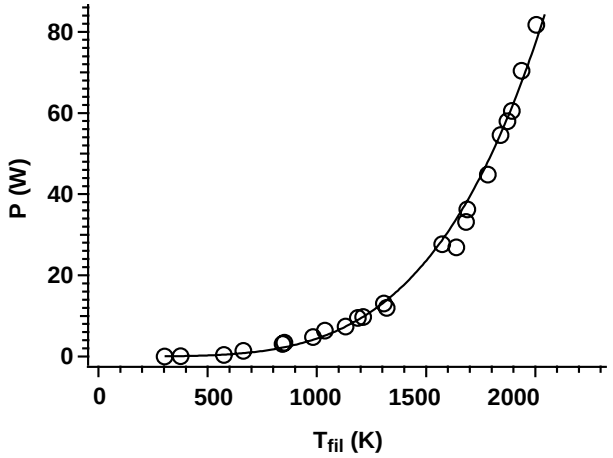

Fig. 3. A plot of electric power consumed by the tungsten filaments vs. the temperature of the filaments.

Fig. 2a and b. The equivalent room temperature resistance of the six tungsten filaments is calculated to be $0.0142\,\Omega$ from their dimensions and resistivity. Therefore, the internal resistance of the rest of the circuit is $0.0633\,\Omega$, the difference of the total resistance from the filaments equivalent resistance at room temperature. Although the filament resistance is only ~20% of the total circuit resistance, the overall temperature of the rest of the circuit is not expected to change significantly due to the large thermal mass and significant heat conductivity of much of the circuit. Thus, the internal resistance is expected to be roughly constant. This internal resistance value ($0.0633\,\Omega$) is subtracted from the total resistance values to obtain the approximate filaments resistance values at different electric power inputs. With the dimensions and resistance of the tungsten filaments, T_{fil} is determined for various power input values using Eq. (1).

Electric power consumed by the filaments is plotted against the T_{fil} in Fig. 3. The power consumption of the filaments is determined from the resistance of the tungsten filaments and the measured electric current. A least-squares fits of these data results in a relationship between power and T_{fil} given by Eq. (2a). Taking into account of the tungsten filaments area, the power consumption of the filaments per unit area is expressed in Eq. (2b):

$$P\,(\text{W}) = 1.9 \times 10^{-12} T_{\text{fil}}^{4.12} \quad (2a)$$

$$\frac{P}{A}\,(\text{W m}^{-2}) = 6.7 \times 10^{-9} T_{\text{fil}}^{4.12} \quad (2b)$$

Both of the above equations resemble the Stefan–Boltzmann law (Eq. (3)) in which the excitance is proportional to temperature to the fourth power:

$$M\,(\text{W m}^{-2}) = 5.67 \times 10^{-8} T^4 \quad (3)$$

where M is the excitance, the photon power emitted from a blackbody source per unit area.

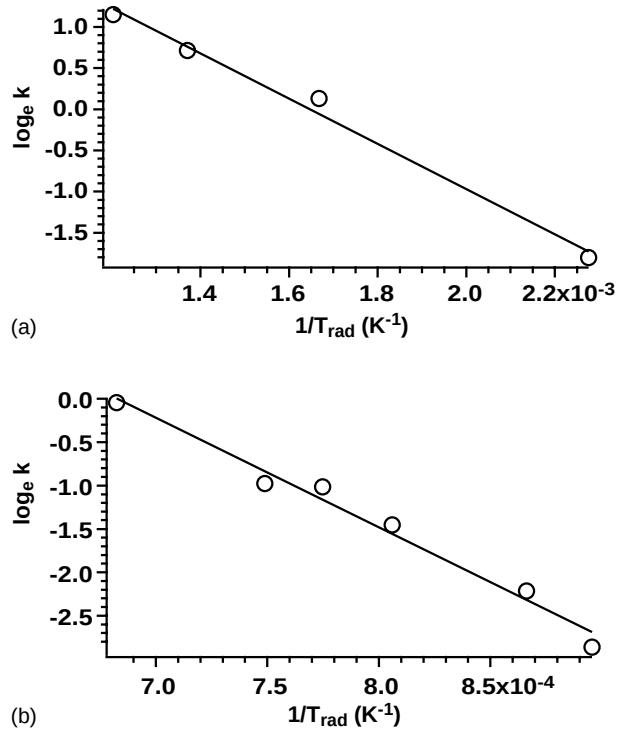

Fig. 4. Arrhenius plots using the radiation temperature for molecular ions of (a) acetophenone and (b) *n*-butylbenzene.

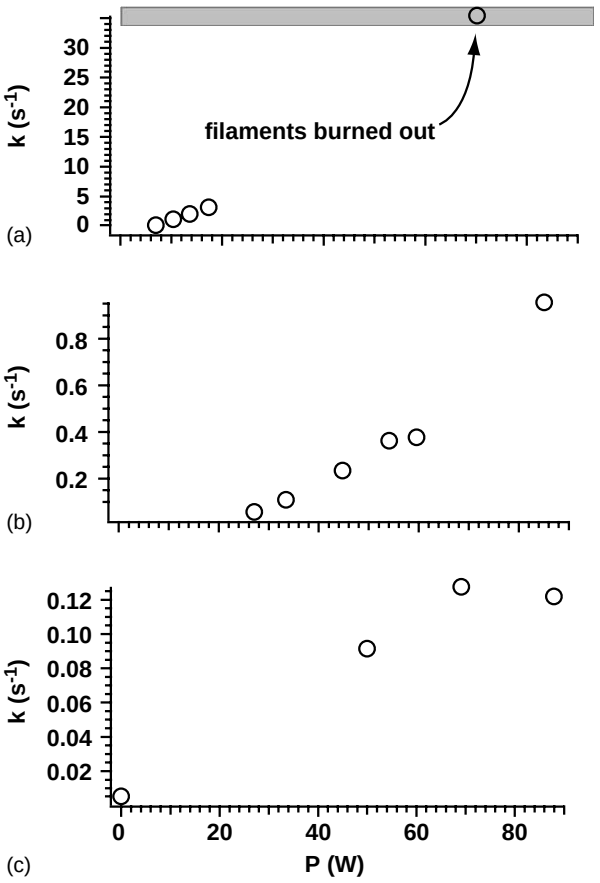

Fig. 5. The dissociation rate constants plotted as function of the applied electric power to the tungsten filaments for (a) acetophenone and (b) *n*-butylbenzene molecular ions inside a 297 K (24 °C) vacuum chamber, and (c) protonated leucine enkephalin inside a 447 K vacuum chamber. For acetophenone molecular ions, the radiation temperature corresponding to the highest rate constant, $35\,s^{-1}$, is unknown because one or more filament(s) burned out.

The pre-exponential factor in Eq. (2b) is smaller than that of Eq. (3) because the emissivity of tungsten at 500–2000 K ranges from 0.053 to 0.26 [31], which corresponds well with the observed one-order magnitude difference. The agreement is better than expected, as P (W) refers to the power dissipated by the tungsten filaments through both photon emission and thermal conduction processes, whereas Stefan–Boltzmann law describes only the photon emission power from a blackbody source.

3.2. Acetophenone molecular ions

For our experiment, the dissociation kinetics of acetophenone molecular ions, $C_6H_5COCH_3^{\bullet+}$, are studied at four radiation temperatures (T_{rad}) ranging from 440 to 830 K. The only dissociation pathway observed is shown in reaction scheme 4.

$$C_6H_5COCH_3^{\bullet+} \rightarrow C_6H_5CO^+ + {}^{\bullet}CH_3 \quad (4)$$

A plot of the $\log_e k_{diss}$ versus the $1/T_{rad}$ is linear. From the slope of these data, a value of the dissociation E_a of 0.24 ± 0.02 eV is obtained (Fig. 4a). Modeling indicates that the Arrhenius data for this ion should be nearly linear over this wide temperature range if the ions are in the truncated Boltzmann limit over the entire range. Using master equation modeling, the E_o is calculated to be 0.46 ± 0.06 eV for various transition state entropies ranging $A^{\infty} = 10^9$–$10^{17}\,s^{-1}$. The limited dependence of the E_o values for the wide range of transition state entropies used indicates the dissociation of this molecular ion is limited by the rate of photon absorption (the "sudden death" limit). These results are very different from those obtained by Sena and Riveros, where they measured an $E_a = 0.48 \pm 0.02$ eV, and calculated a value of $E_o = 0.83 \pm 0.02$ eV [24]. Previously measured E_o values ranging from 0.39 to 0.88 eV have been reported [32–35]. Although the E_a and E_o values reported here are significantly different than those reported by Sena and Riveros, the E_o values from both experiments fit within this wide range of previously reported values.

In Fig. 5a, the k_{diss} for acetophenone molecular ions is plotted as a function of electric power consumed by the heated tungsten filaments. The value of k_{diss} increases roughly linearly with electric power, a result also reported by Sena and Riveros [24]. The data point associated with the highest k_{diss} in Fig. 5a is not used to determine E_a be-

cause at that power, one or more of the tungsten filament(s) burned out. That data point is included in Fig. 5a to indicate the potential of this device to induce very rapid dissociation of ions, much higher than what has been previously reported using heated filaments. The highest k_{diss} induced by our heated filament device for acetophenone molecular ions is $\sim 35\,s^{-1}$, which is ~8 times greater than the highest k_{diss} value ($\sim 4.5\,s^{-1}$) reported by Sena and Riveros [24]. Moreover, we find that a much higher k_{diss} value is obtained for acetophenone at a given T_{rad} with our experimental setup. For example, acetophenone molecular ions dissociate with a $k_{diss} = 3.16\,s^{-1}$ at $T_{rad} = 830\,K$ in our device, and dissociate with a k_{diss} $\sim 0.29\,s^{-1}$ at $T_{rad} = 910\,K$ in their device. The higher dissociation efficiency of our experimental apparatus is attributed to the greater numbers of filaments, thus greater heated surface area and a greater solid angle exposure to the filaments, which produce a higher photon flux.

There are two likely reasons for the different E_a values obtained here and by Sena and Riveros [24]. First, errors in determining the T_{rad} will alter the slope of the resulting Arrhenius plot. Second, under the condition of this experiment, the measured Arrhenius E_a value is likely to depend on photon flux which depends on the experimental setup. In our device, the six tungsten filaments make up ~1% of the total surface area of the ion cell. Because the light transmission of the mesh screen is only ~25%, the photon intensity in the ion cell is attenuated to ~0.25% of the incident photon intensity off the filaments. The faster acetophenone dissociation measured here at a lower T_{rad} than that obtained by Sena and Riveros [24] indicates a higher solid angle exposure to the filaments in our experiment. The estimated solid angle exposure is a lower limit to the photon flux because photons produced by the heated filaments can be reflected within the ion cell and be absorbed by the ions, thus increasing the overall photon flux. In addition, heating of the ion cell by the hot filaments will produce background radiation above room temperature. Sena and Riveros [24] proposed that the measured E_a is insensitive to the solid angle exposure for value above 6%. It is not clear that this criterion is satisfied by either experimental apparatus which raises doubt regarding the measured E_a.

3.3. n-Butylbenzene molecular ions

The branching ratio of *m/z* 91 and 92 formed by dissociation of molecular ions of *n*-butylbenzene, $C_6H_5(CH_2)_3CH_3^{\bullet +}$, has been used to determine the internal energy of the parent ions (reaction scheme 5) [16,36,37]. The dissociation pathway for formation of *m/z* 92 has a lower E_o value and a tighter transition state than the dissociation pathway for formation of *m/z* 91. Dunbar and coworker have measured E_o of 1.1 eV for the dissociation of *n*-butylbenzene molecular ions to *m/z* 92 and 1.7 eV to *m/z* 91 [16]. Baer et al. have measured E_o values of 0.99 and 1.6 eV and $\Delta S^{\ddagger}$ values of −7 and +3.5 cal/K mol for formation of *m/z* 92 and 91, respectively [37]:

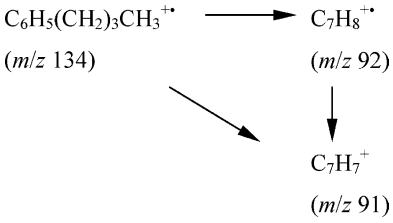

(5)

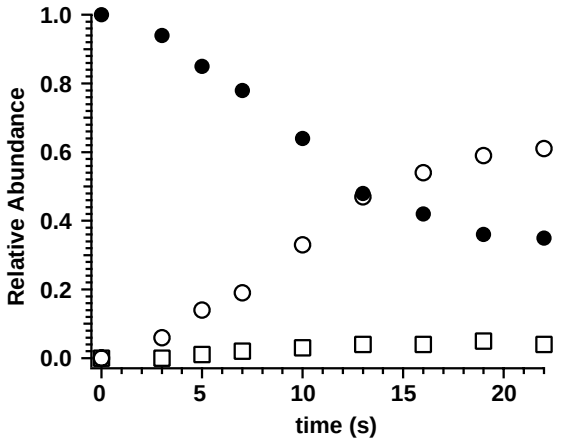

Fig. 6. Relative abundance of *n*-butylbenzene molecular ions (●) and its dissociation product ions at *m/z* 91 (□) and 92 (○) plotted as a function of time at radiative temperature 1120 K.

Dissociation of *n*-butylbenzene molecular ions is studied at the T_{rad} ranging from 1120 to 1480 K using our heated filament apparatus. In Fig. 6, the relative abundances of the reactant and product ions are plotted as a function of reaction time wih $T_{rad} = 1120\,K$. The k_{diss} is $0.057\,s^{-1}$ and the abundance of *m/z* 91 is roughly 6% that of *m/z* 92. As was the case for acetophenone molecular ions, the k_{diss} of *n*-butylbenzene molecular ions is approximately linear with the electric power supplied to filaments (Fig. 5b).

Fig. 4b is an Arrhenius plot for *n*-butylbenzene using T_{rad}. From this plot, an E_a of 1.09 ± 0.08 eV is obtained. Formation of *m/z* 92 occurs via a McLafferty rearrangement, and its transition state entropy change ($\Delta S^{\ddagger}$) of −7 cal/K mol [37] corresponds to an Arrhenius A^{∞} factor of $5 \times 10^{11}\,s^{-1}$. Values of A^{∞} ranging from 10^9 to $10^{13}\,s^{-1}$ were used in the master equation modeling. From the modeling, an E_o value of 2.1 ± 0.3 eV is obtained. This value is much higher than most previously reported values, indicating a significant problem with our analysis of these data. It is interesting to note that the E_o value we obtain for the acetophenone molecular ion is about half of that reported by Sena and Riveros [24], but the E_o value we obtain for *n*-butylbenzene is nearly twice as large as previously reported values [16,37].

To better understand the energy deposition due to the heated filaments, dissociation data for *n*-butylbenzene molecular ion were compared to those obtained by BIRD at 467 K (194 °C). The BIRD k_{diss} of *n*-butylbenzene molecular ion for formation of product *m/z* 92 is $\sim 0.003\,s^{-1}$;

no m/z 91 is observed. By comparison, the fastest k_{diss} we obtained using the heated filament cell is more than 300 times greater ($0.96\,s^{-1}$) (Fig. 4b). Extrapolating from the Arrhenius plot of Fig. 4b, the k_{diss} of $\sim 0.003\,s^{-1}$ from the 467 K BIRD experiment can be reproduced using the heated filament device at $T_{rad} = 875$ K. This result clearly demonstrates that the heated filament apparatus can easily increase the "effective" internal energy of *n*-butylbenzene molecular ions significantly above that obtained at 467 K with BIRD. Note that this "effective temperature" is not the same as a true Boltzmann distribution because of depletion of the population at the higher internal energies, which occurs with both the filament dissociation and with BIRD for this ion. Based on the E_o and $\Delta S^{\ddagger}$ measured by Baer et al. [37], a rate constant increase from 0.003 to $0.96\,s^{-1}$ corresponds to an elevation of a true temperature of 80 K.

The appearance of m/z 91 in the heated filament dissociation experiment is interesting because this dissociation pathway does not become competitive with that of m/z 92 until the internal energy of the reactant ions is 2–3 eV [16,37]. Baer and coworkers reported that the k_{diss} for formation of m/z 92 at an internal energy of 2.0 eV is on the order of 10^5–$10^6\,s^{-1}$. Yet, the observed k_{diss} to m/z 92 in this experiment (Fig. 6) is only $0.057\,s^{-1}$, which indicates an "effective" temperature too low to provide measurable m/z 91.

Uechi and Dunbar have demonstrated that CO_2 laser irradiation of the molecular ions of *n*-butylbenzene yielded exclusively m/z 92 [19,38]. The highest IRMPD induced k_{diss} in their experiment is $10.5\,s^{-1}$ [19], which is much greater than the highest k_{diss} in this experiment ($0.96\,s^{-1}$). Therefore, absorption at the infrared frequencies alone does not explain the appearance of m/z 91 in our experiment. This indicates that the appearance of m/z 91 must be the result of higher energy photons, e.g., visible photons, from the heated filaments.

The appearance energy of m/z 91 is 1.6 eV, an energy equivalent to a visible photon at 775 nm. The photon distribution inside an ion cell with a heated filament is very much like a high temperature blackbody distribution except the photon intensity is attenuated. Consequently, the heated filament device can provide significant amount of visible photons which have sufficient energy to produce m/z 91, while maintaining the overall dissociation rate constant of *n*-butylbenzene low. For example, the integrated photon energy density of wavelengths shorter than 775 nm in a 1500 K blackbody field is 10^{22} times of that in a 298 K blackbody field, but the total integrated energy density (all wavelengths) in a 1500 K blackbody field is only 640 times that in a 298 K blackbody field. Fig. 7 illustrates Planck distributions at temperatures of 297 K and that of 1500 K (the latter is attenuated by a factor of 10^3). As can be clearly seen, a 1500 K source emits significantly more energy at wavelengths shorter than 5000 nm.

Thus, it appears that our inability to obtain a good value of E_o for dissociation of the *n*-butylbenzene ions is due in part to not including visible wavelengths in our modeling process. In addition, we use T_{rad} in our modeling which provides the correct total emission power but not the correct wavelength distribution. A better way to do this would be to use a color temperature appropriate to the corresponding filament temperature normalized to the emissivity of the filament and the attenuation due to the geometry of the experimental setup.

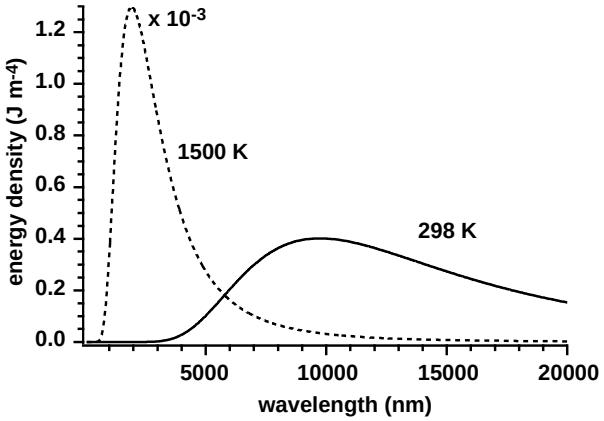

Fig. 7. Planck distributions at 298 K (solid line) and at 1500 K (dash line). The energy density of the Planck distribution at 1500 K has been reduced by 1000 times.

3.4. Protonated leucine enkephalin

The dissociation pathways and energetics of protonated leucine enkephalin [Tyr-Gly-Gly-Phe-Leu + H]$^+$ have been previously investigated [12,39–41]. With the heated filament device, protonated leucine enkephalin remains intact after being exposed to $T_{rad} = 1480$ K for 10 s. However, the protonated peptide undergoes observable dissociation at 437 and 447 K (164 and 174 °C) with BIRD (Fig. 8a and b). A upper limit to k_{diss} due to the heated filaments at $T_{rad} = 1480$ K is $< 6 \times 10^{-4}\,s^{-1}$. Using Arrhenius parameters obtained from the BIRD experiments, the "effective" temperature of the ions exposed to the heated filaments at $T_{rad} = 1480$ K is less than 417 K (144 °C). In contrast, *n*-butylbenzene molecular ions had an "effective" temperature greater than 467 K (194 °C) when the heat filaments were at $T_{rad} = 1120$ K. Thus, the filaments are producing significantly different internal energies of the two ions.

The dissociation of doubly protonated bradykinin was also investigated using a slightly different heated filaments device in which the tungsten filaments were longer. About 11% of the doubly protonated ion dissociate after 10 s at the maximum power to form complementary b_2/y_7 fragment ions and loss of water. The "effective" temperature of the ion is estimated to be 426 K (153 °C) based on Arrhenius values obtained from previous BIRD experiments [10], which corresponds to a ~120 °C increases from the slightly heated 35 °C ion cell.

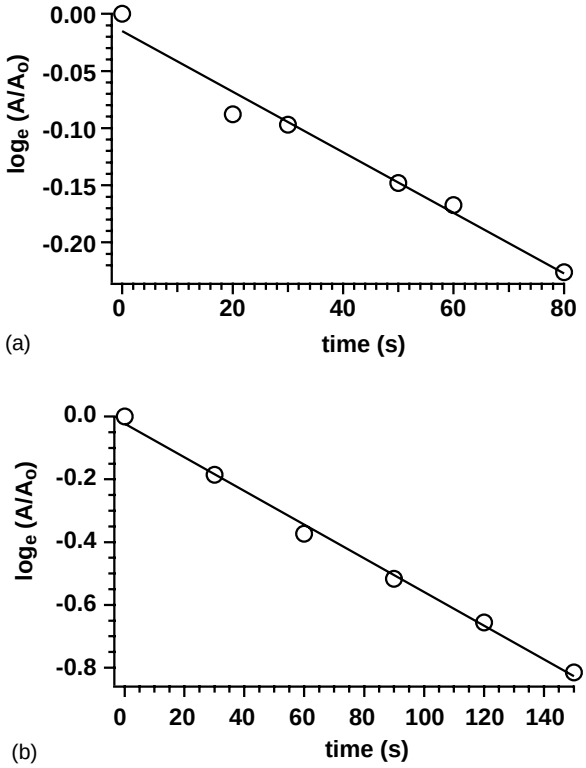

Fig. 8. First-order kinetic plots for the dissociation of protonated leucine enkephalin obtained by BIRD at (a) 437 K and (b) 447 K.

One possible explanation for the different "effective" temperature *n*-butylbenzene molecular ions, protonated leucine enkephalin and doubly protonated bradykinin in these heated filaments experiment is that the protonated peptides have greater numbers of vibrational frequencies so that radiative emission is more efficient. A small ion that absorbs a visible photon can dissociate on a time scale faster than radiative emission. In contrast, the dissociation rate upon absorption of a single visible photon will decrease with increasing ion size for a given dissociation process (the degree of freedom effect). Moreover, rates of radiative emission and absorption increase with increasing molecular size. Thus, larger ions can rapidly loose the energy corresponding to the absorption of a single visible photon either by emission of a visible photon or of multiple infrared photons before it has time to dissociate, i.e., it is closer to the rapid energy exchange limit [13]. As a result, large and small ions can equilibrate to different effective internal temperatures. If ions equilibrate differently to the filament radiation, Arrhenius E_a values based on the T_{rad} are difficult to interpret.

To determine how much energy is being transferred into protonated leucine enkephalin, the peptide ions were dissociated with a combination of heated filaments and BIRD with the vacuum chamber temperature at 447 K. In Fig. 5c, the k_{diss} is plotted as a function of electric power consumed by the tungsten filaments. Radiation temperatures of 447, 1810, 1950 and 2060 K are obtained at 0, 50, 69 and 88 W, respectively. The k_{diss} of protonated leucine enkephalin is clearly affected by the radiation temperature of the filaments (Fig. 5c).

The total energy density, ε (J m^{-3}), in a blackbody radiation field is proportional to the fourth power of the temperature T (K) (Eq. (6)),

$$\varepsilon = aT^4 \tag{6}$$

where a is equal to 7.56×10^{-16} J m^{-3} K^{-4}.

With the filaments off, the k_{diss} is represented by the 447 K blackbody photon distribution. With 50, 69, and 88 W supplied to the filaments, the resulting k_{diss} values are equal to those from 492, 498 and 497 K BIRD experiments, respectively (Fig. 5c). Thus, the additional electric power to the tungsten filaments is responsible for the elevation in the effective temperature of protonated leucine enkephalin. The energy densities in the 447, 492, 498 and 497 K blackbody radiative field are calculated using Eq. (5). The energy density difference between 447 and 497 K, 1.42×10^{-5} J m^{-3}, is due to the application of 50 W to the filaments. Assuming emission power increases linearly with supplying electric power, supplying 110 W to our filaments device can induce a k_{diss} of protonated leucine enkephalin similar to that obtained at 447 K with BIRD. For 69 and 88 W filament power data, the extrapolated powers are 130 and 170 W, respectively. Although there is significant scatter in these data, we conclude that a filament power between 110 and 170 W is necessary to significantly dissociate protonated leucine enkephalin without heating the vacuum chamber, which corresponds to a 2–3-fold increase in maximum power or light transmittance over that obtained in our current experimental setup.

4. Conclusions

The capabilities of a new heated filament apparatus for dissociating ions in a FT-ICR mass spectrometer are demonstrated. For small ions, we find faster dissociation than what has been reported previously due to the higher power capabilities of this apparatus. We find that the "effective" internal temperature of small ions can be raised significantly above 470 K. We also find that higher energy fragmentation pathways can be observed over those observed using just infrared radiation, either blackbody or CO_2 laser photodissociation. These results can only be rationalized by the absorption of visible photons emitted by the filaments, with temperatures estimated to be as high as 2000 K with the current apparatus. An Arrhenius plot in which the natural log of the dissociation rate constant is plotted as a function of the inverse radiation temperature ($\log_e k_{diss}$ versus $1/T_{rad}$) results in a linear relationship from which one can obtain an Arrhenius activation energy. However, obtaining a value of the threshold dissociation from this E_a value is difficult due to differences in photon absorption and emission as well as dissociation for different ions and because we do not include absorption or emission of visible photons in our modeling.

In contrast to the small ions, larger protonated peptide ions do not dissociate significantly using the heated filaments. The "effective" internal temperature of protonated leucine enkephalin is only raised by ∼50 °C at the highest powers used, although with a different heated filament ion cell, the "effective" temperature of the doubly protonated bradykinin could be raised ∼120 °C. To obtain the equivalent dissociation of a 467 K BIRD experiment for protonated leucine enkephalin, we estimate that between 110 and 170 W would be necessary in the current apparatus. This represents a 2–3 fold increase in photon flux. The simplest way to obtain this increase would be to replace the woven copper meshes that are in front of the filaments, which have 25% transmittance, with electroformed meshes that can have ∼90% transmittance. To obtain even higher photon fluxes, the distance between the filaments and the center of the cell could be reduced by making the cell smaller. Additional filaments could be added to the cell and all conducting surfaces in the region of the cell could be polished and coated with gold to increase the reflectivity of the surfaces. With these modifications, it should be possible to readily dissociate biological ions in a short time frame. This method has several potential advantages over other slow heating methods, such as SORI-CAD, including no increased gas load, fast and reproducible dissociation kinetics, and the potential to extract thermochemical information from the dissociation data measured at multiple filament temperatures.

Acknowledgements

The authors would like to thank Professor Robert C. Dunbar for helpful discussions and Mr. Kolja Paech for assistance. This research would not have been possible if not for the generous financial support provided by National Science Foundation (grant CHE-0098109).

References

[1] M.J. Coggiola, P.A. Schulz, Y.T. Lee, Y.R. Shen, Phys. Rev. Lett. 38 (1977) 17.
[2] A.S. Sudbo, P.A. Schulz, E.R. Grant, Y.T. Lee, J. Chem. Phys. 68 (1977) 1306.
[3] R.L. Woodin, D.S. Bomse, J.L. Beauchamp, J. Am. Chem. Soc. 100 (1978) 3248.
[4] D.S. Bomse, R.L. Woodin, J.L. Beauchamp, J. Am. Chem. Soc. 101 (1979) 5503.
[5] R.N. Rosenfeld, J.M. Jasinski, J.I. Brauman, J. Am. Chem. Soc. 101 (1979) 3999.
[6] J.M. Jasinski, R.N. Rosenfeld, F.K. Meyer, J.I. Brauman, J. Am. Chem. Soc. 104 (1982) 652.
[7] G. Baykut, C.H. Watson, R.R. Weller, J.R. Eyler, J. Am. Chem. Soc. 107 (1985) 8036.
[8] R.C. Dunbar, T.B. McMahon, D. Tholmann, D.S. Tonner, D.R. Salahub, D. Wei, J. Am. Chem. Soc. 117 (1995) 12819.
[9] W.D. Price, P.D. Schnier, E.R. Williams, Anal. Chem. 68 (1996) 859.
[10] P.D. Schnier, W.D. Price, R.A. Jockusch, E.R. Williams, J. Am. Chem. Soc. 118 (1996) 7178.
[11] W.D. Price, P.D. Schnier, R.A. Jockusch, E.F. Strittmatter, E.R. Williams, J. Am. Chem. Soc. 118 (1996) 10640.
[12] P.D. Schnier, W.D. Price, E.F. Strittmatter, E.R. Williams, J. Am. Soc. Mass Spectrom. 8 (1997) 771.
[13] W.D. Price, E.R. Williams, J. Phys. Chem. A 101 (1997) 8844.
[14] W.D. Price, P.D. Schnier, E.R. Williams, J. Phys. Chem. B 101 (1997) 664.
[15] D.P. Little, J.P. Speir, M.W. Senko, P.B. O'Connor, F.W. McLafferty, Anal. Chem. 66 (1994) 2809.
[16] J.H. Chen, J.D. Hays, R.C. Dunbar, J. Phys. Chem. 88 (1984) 4759.
[17] R.C. Dunbar, J. Chem. Phys. 95 (1991) 2537.
[18] R.C. Dunbar, R.C. Zaniewski, J. Chem. Phys. 96 (1992) 5069.
[19] G.T. Uechi, R.C. Dunbar, J. Chem. Phys. 96 (1992) 8897.
[20] M.A. Freitas, C.L. Hendrickson, A.G. Marshall, Rapid Commun. Mass Spectrom. 13 (1999) 1639.
[21] M.A. Freitas, C.L. Hendrickson, A.G. Marshall, J. Am. Chem. Soc. 122 (2000) 7768.
[22] R.A. Jockusch, K. Paech, E.R. Williams, J. Phys. Chem. A 104 (2000) 3188.
[23] K. Paech, R.A. Jockusch, E.R. Williams, J. Phys. Chem. A 106 (2002) 9761.
[24] M. Sena, J.M. Riveros, J. Phys. Chem. A 101 (1997) 4384.
[25] M. Sena, J.M. Riveros, Chem. Eur. J. 6 (2000) 785.
[26] T. Giroldo, J.M. Riveros, J. Phys. Chem. A 106 (2002) 9930.
[27] M. Sena, J.M. Riveros, Int. J. Mass Spectrom. 227 (2003) 135.
[28] S.M. Peterman, B.K. Bluhm, D.H. Russell, Dissociation dynamics of $C_7H_7Cl^+$-thermal activation and theory, in: Proceedings of the 46th ASMS Conference on Mass Spectrometry and Allied Topics, 1998, Orlando, FL.
[29] G.A. Janaway, J.I. Brauman, J. Phys. Chem. A 104 (2000) 1117.
[30] R.L. Wong, K. Paech, E.R. Williams, Int. J. Mass Spectrom. 232 (2004) 59.
[31] W.E. Forsythe, Temperature, brightness and efficiency of selected sources of light, in: E.W. Washburn (Ed.), International Critical Tables of Numerical Data, Physics, Chemistry and Technology, vol. 5, McGraw-Hill Book Company, New York, 1929, p. 242.
[32] F.W. McLafferty, P.F.I. Bente, R. Kornfeld, S.-C. Tsai, I. Howe, J. Am. Chem. Soc. 95 (1972) 2010.
[33] F. Benoit, Org. Mass Spectrom. 7 (1973) 1407.
[34] J.F. Elder, J.H. Beynon, R.G. Cooks, Org. Mass Spectrom. 11 (1976) 415.
[35] R.G. McLoughlin, J.C. Traeger, Org. Mass Spectrom. 14 (1979) 434.
[36] P. Brown, Org. Mass Spectrom. 3 (1970) 1175.
[37] T. Baer, O. Dutuit, H. Mastdagh, C. Rolando, J. Phys. Chem. 92 (1988) 5674.
[38] G.T. Uechi, R.C. Dunbar, J. Chem. Phys. 98 (1993) 7888.
[39] P.D. Schnier, J.J. Jurchen, E.R. Williams, J. Phys. Chem. B 103 (1999) 737.
[40] K.G. Asano, D.J. Butcher, D.E. Goeringer, S.A. McLuckey, J. Mass Spectrom. 34 (1999) 691.
[41] D.E. Goeringer, K.G. Asano, S.A. McLuckey, Int. J. Mass Spectrom. 183 (1999) 275.